Chapter 5

Transportation of micro-polar fluids by means of dilating peristaltic waves in a tube of non-uniform cross-sectional area: Application to sliding hiatus hernia

The contents of this chapter have been published in **Journal of Physics: Conf. Series 1141**, 012092 (2018).

5.1 Introduction

A peristaltic pump is a device for pumping fluids, generally from a region of lower to higher pressure, by means of a contraction wave travelling along a tube-like structure. This travelling-wave phenomenon is referred to as "peristaltis". Peristalsis originated naturally as a means of pumping physiological fluids from one place in the body to another and is the primary pumping mechanism in swallowing (and indeed all the way through the alimentary canal) (cf. J. G. Brasseur (1987)). Examples include the movement of food through the digestive system, passage of urine from the kidney to the bladder. Peristaltic transport deals with a given train of waves moving with invariable speed on the elastic boundaries. It pumps bio-fluids against the pressure rise. Peristaltic waves occur in the oesophagus, stomach, vas deferens, fallopian tube, intestines and in many other parts of human body. A major industrial and clinical application of this principle is in the design of the diabetic pump, blood pumps in heart- lung machines, roller and finger pumps. It also has other industrial applications such as transport of corrosive fluids and sanitary fluid transport for which contact of the fluid with the machinery components is forbidden.

The dome-shaped muscle which separates the abdomen and chest is called diaphragm. The oesophagus passes through an opening (the hiatus) in the diaphragm to connect to the stomach. When elements of the abdominal cavity bulge up through the oesophageal hiatus into the part of the thoracic cavity between the lungs, it is called hiatus hernia (Figure 5.1). One of the recognized theories of the origin of this hiatus hernia is that intra-abdominal pressure increases above the normal value to increase the normal gradient between intra-thoracic and intra-abdominal pressure. Consequently, the oesophagogastric junction is

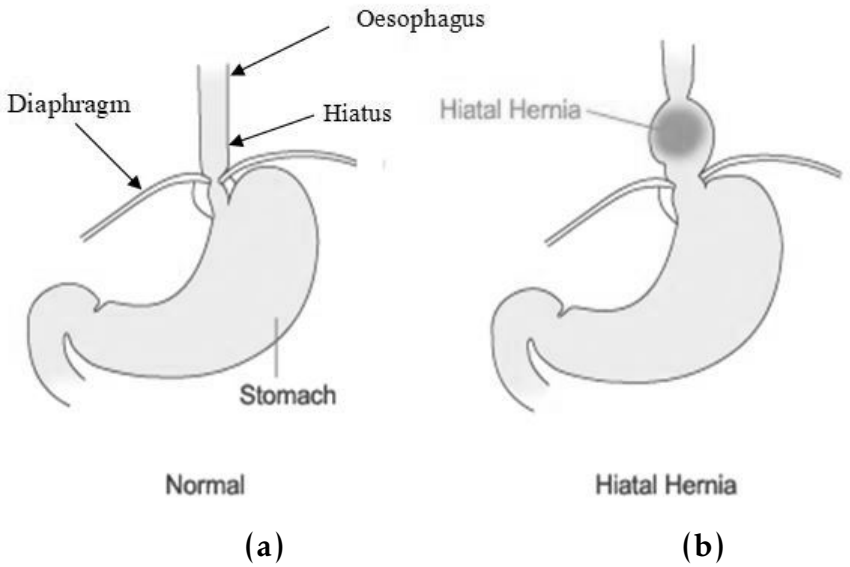

Figure 5.1: Diagrams for (a) Normal oesophagus and (b) Oesophagus suffering from sliding hiatus hernia. (Source of figure 5.1 https://www.melbournegastrosurgery.com.au/surgery-for-gastric-reflux-hiatus-hernia/)

pushed up into hiatus (cf. Christensen and Miftakhov (2000)). Due to this herniation oesophagus diverges at the distal end. This model investigates the effect of this divergence of oesophagus on swallowing of such food stuffs which have micropolar fluid nature.

We focus our study on sliding hiatus hernia which is very common and is defined as a significant axial prolapsed of a portion of the stomach through the diaphragmatic oesophageal hiatus. It is usually described as a more than 2 cm separation of the upward displaced oesophagogastric junction and diaphragmatic impression (cf. Weyenberg (2013)).

The lower oesophageal sphincter is a thickened area of the circular muscle layer of the distal oesophagus, in humans extending over an axial length of 2 -

4 cm. The main function of the lower oesophageal sphincter is to generate a high-pressure zone to save from harm the oesophagus against reflux from caustic gastric contents. During swallowing or belching, its muscle must relax temporarily in order to permit passage of ingested food or intra-gastric air. Swallow-induced relaxation is part of primary peristalsis (cf. Boeckxstaens (2005)).

Micro polar fluids contain micro constituents which can undergo rotation, the presence of which can affect the hydrodynamics of the flow such that it can be distinctly non-Newtonian. Physically, micro polar fluids may represent fluids consisting of rigid, randomly oriented (or spherical) particles suspended in a viscous medium, where the deformation of fluid particles is ignored (cf. Grzegorz Lukaszewicz). Micro-polar fluids are the very common type of fluids such as blood, some edible solutions, polymer solutions, colloidal solutions, drilling fluids in oil industries, some food materials such as the solutions of roasted cereal powders consumed in Indian sub continent (cf. Bourne (2002)).

The study of the mechanism of peristalsis, in mechanical and physiological situation has been the object of scientific research from the long time. Since the first investigation of Latham (1966), several theoretical and experimental attempts have been made to understand peristaltic action in different situations. In the early studies of peristalsis, most of the theoretical investigations and clinical observations took time to gain momentum (cf. (1968), (1969)). These investigations are carried out by considering fluid as Newtonian and tube or channel as having uniform cross-sectional area. With the development of medical and physical sciences, it has been recognized that the bio-fluids do not behave like Newtonian fluids and fail to give a better understanding when a peristaltic mechanism is involved in small blood vessels, intestine, transport of spermatozoa in the cervical canal. It has now been accepted that most of the physiological fluids behave

like the non-Newtonian fluids. Peristalsis in a male reproductive system was observed experimentally and numerically by Batra (1974), Guha *et al*. (1975), Gupta *et al*. (1976) and Srivastava *et al*. (1985). Guha *et al*. (1975) studied the transport of the spermatic fluid in the vas deferens of monkey and reported that the transportation during ejaculation is mainly due to contraction of the ampulla and filling during the non-ejaculatory phase is due to peristalsis and epididymal pressure. Srivastava *et al*. (cf. (1985), (1982)) modelled the peristaltic flow in the vas deferens by considering it a non-uniform diverging tube and a channel. They examined a more realistic model by investigating power-law fluid flow in a non-uniform tube and blood as a Casson fluid flowing inside small capillaries and blood vessels. Misra and Pandey (1995) modelled axisymmetric peristaltic motion of a Newtonian viscous incompressible fluid through a flexible tube of changing cross-section, where the nonlinear convective acceleration terms were supposed to be not negligible compared to the viscous terms. Their reports were more ascribable than the previous reports for spermatic flow reported by Guha *et al*. (1975). Eytan *et al*. (cf. (1999), (2001)) investigated the effect of peristalsis in embryo transport within the uterine cavity. They discussed in detail the phenomenon of trapping and how the particle reflux impedes the embryo implantation at the fundus. Hariharan *et al*. (2008) studied the peristaltic transport of non-Newtonian fluid in a diverging tube with different waveforms and concluded that square wave has the best pumping characteristics of all the wave forms and the triangular wave has the worst characteristics.

Li and Brasseur (1993) studied the transport of food bolus in the oesophagus with integral and non-integral number of waves. Misra and Pandey (2001) gave a more suitable model with modified wall equation for oesophageal swallowing. Pandey and Chaube (cf. (2011), (2010)) investigated the peristaltic

transport of Maxwell and viscoelastic fluid in a channel and a tube of varying cross sections respectively. Kahrilas *et al*. (1995) reported an experimental investigation of high- pressure zone located in the lower part of the oesophagus whose length varies from a normal oesophagus to an oesophagus which suffers from a hiatus hernia. In another experimental investigation, Xia *et al*. (2009) measured oesophageal wall thickness in contracted and dilated states through CT images of adult patients without oesophageal diseases. On the basis of this, Pandey *et al*. (2017) concluded that in the dilated state the upper oesophagus is thicker while in the contracted state the lower oesophagus is thicker and modelled the oesophageal swallowing with peristaltic waves of exponentially increasing wave amplitude for a Newtonian fluid. Several kinds of literature are available that explain the mathematics of peristalsis and its effect on the fluid flow in a diverging tube with non-Newtonian fluid. This investigation is different from those of previous investigations. Because, due to sliding hiatus hernia the cross-sectional area of the oesophagus does not keep on uniform throughout its length, and consequently, it gets diverged at the distal end. Sometime it may be diverged and then converged near the distal end. In light of this, the purpose of the present analysis is to put forward the effect of sliding hiatus hernia on the oesophageal swallowing with dilating peristaltic wave amplitude for non-Newtonian fluid (micro-polar fluid).

5.2 Mathematical Formulation

We consider the flow of micro-polar fluid in a tube of length of $\tilde{l}$ caused by continuous contraction waves that propagate on the walls of the tube (cf. Figure 5.2) and are given by

$$\tilde{h}(\tilde{x},\tilde{\omega},\tilde{t}) = a + \tilde{b}\tilde{x} - \tilde{\phi}\, e^{\tilde{\omega}\tilde{x}} \cos^2 \frac{\pi}{\lambda}(\tilde{x} - c\tilde{t}), \tag{5.1}$$

where $\tilde{h}$, $\tilde{x}$, $\tilde{t}$, a, $\tilde{b}$, $\tilde{\phi}$, λ, $\tilde{\omega}$ and c respectively stand for radial displacement of the wall, axial coordinate, time, radius of the tube, constant whose magnitude depend on the length of the tube or gradient parameter, amplitude of the wave, wavelength, damping parameter and wave velocity.

The governing equations of the flow of micro-polar fluid in the absence of body forces and body couple are given by

$$\frac{\partial \tilde{u}}{\partial \tilde{x}} + \frac{1}{\tilde{r}}\left(\frac{\partial(\tilde{r}\tilde{v})}{\partial \tilde{r}}\right) = 0, \tag{5.2}$$

$$\rho\left(\frac{\partial \tilde{u}}{\partial \tilde{t}} + \tilde{u}\frac{\partial \tilde{u}}{\partial \tilde{x}} + \tilde{v}\frac{\partial \tilde{u}}{\partial \tilde{r}}\right) = -\frac{\partial \tilde{p}}{\partial \tilde{x}} + k\frac{1}{\tilde{r}}\frac{\partial(\tilde{r}\tilde{w})}{\partial \tilde{r}} + (\mu + k)\left(\frac{\partial^2 \tilde{u}}{\partial \tilde{x}^2} + \frac{1}{\tilde{r}}\frac{\partial}{\partial \tilde{r}}\left(\tilde{r}\frac{\partial \tilde{u}}{\partial \tilde{r}}\right)\right), \tag{5.3}$$

$$\rho\left(\frac{\partial \tilde{v}}{\partial \tilde{t}} + \tilde{u}\frac{\partial \tilde{v}}{\partial \tilde{x}} + \tilde{v}\frac{\partial \tilde{v}}{\partial \tilde{r}}\right) = -\frac{\partial \tilde{p}}{\partial \tilde{r}} - k\frac{\partial \tilde{w}}{\partial \tilde{x}} + (\mu + k)\left(\frac{\partial^2 \tilde{v}}{\partial \tilde{x}^2} + \frac{\partial}{\partial \tilde{r}}\left(\frac{1}{\tilde{r}}\frac{\partial(\tilde{r}\tilde{v})}{\partial \tilde{r}}\right)\right), \tag{5.4}$$

$$\rho\tilde{\sigma}\left(\frac{\partial \tilde{w}}{\partial \tilde{t}} + \tilde{u}\frac{\partial \tilde{w}}{\partial \tilde{x}} + \tilde{v}\frac{\partial \tilde{w}}{\partial \tilde{r}}\right) = -2k\tilde{w} + k\left(\frac{\partial \tilde{v}}{\partial \tilde{x}} - \frac{\partial \tilde{u}}{\partial \tilde{r}}\right) + \gamma\left(\frac{\partial^2 \tilde{w}}{\partial \tilde{x}^2} + \frac{\partial}{\partial \tilde{r}}\left(\frac{1}{\tilde{r}}\frac{\partial(\tilde{r}\tilde{w})}{\partial \tilde{r}}\right)\right)$$
$$+ (\alpha + \beta + \gamma)\tilde{\nabla}(\tilde{\nabla}.\tilde{w}). \tag{5.5}$$

where $\tilde{u}$, $\tilde{v}$, $\tilde{w}$, $\tilde{r}$, ρ, $\tilde{\sigma}$ are axial velocity, radial velocity, micro-polar vector, radial coordinate, fluid density, micro-gyration parameter, respectively and μ, k, α, β, γ are material constants and satisfy the following conditions:

$$2\mu + k \geq 0,\ k \geq 0,\ 3\alpha + \beta + \gamma \geq 0,\ \gamma \geq |\ \beta\ |, \tag{5.6}$$

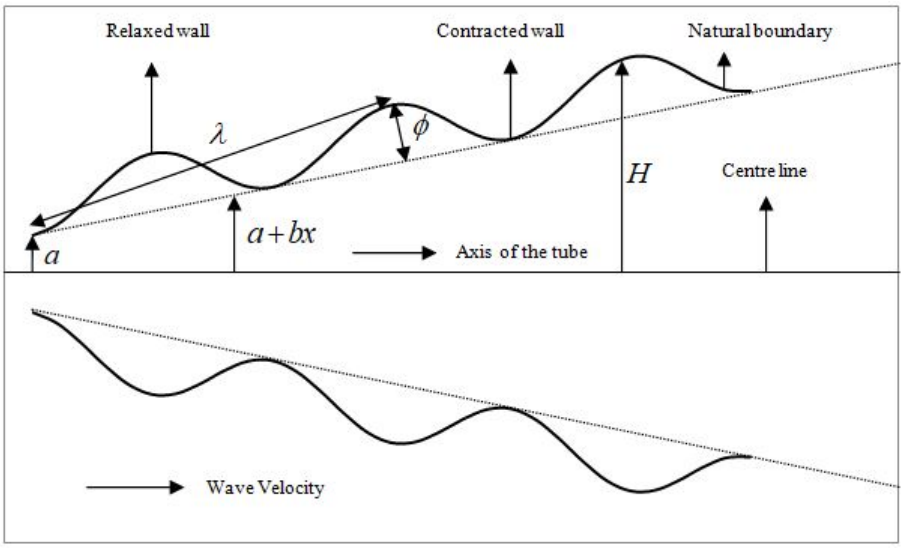

Figure 5.2: The diagram, based on equation (5.12), represents the propagation of a progressive wave along the walls of the tube containing fluid, which undergoes contraction and relaxation but no expansion beyond the boundary.

For the subsequent analysis, the dependent variables are non - dimensionalized as follow.

$$x=\frac{\tilde{x}}{\lambda}, r=\frac{\tilde{r}}{a}, t=\frac{c\tilde{t}}{\lambda}, u=\frac{\tilde{u}}{c}, v=\frac{\tilde{v}}{c\delta}, \delta=\frac{a}{\lambda}, w=\frac{a\tilde{w}}{c}, h=\frac{\tilde{h}}{a}, b=\frac{\tilde{b}\lambda}{a},$$
$$l=\frac{\tilde{l}}{\lambda}, \phi=\frac{\tilde{\phi}}{a}, \sigma=\frac{\tilde{\sigma}}{a^2}, p=\frac{\tilde{p}a^2}{\mu c\lambda}, Re=\frac{\rho ca\delta}{\mu}, Q=\frac{\tilde{Q}}{\pi a^2 c}, \omega=\lambda\tilde{\omega}, \tag{5.7}$$

where $\delta=\frac{a}{\lambda}$ is wave number; Re is the Reynolds number and Q is volume flow rate.

After introducing the non dimensional parameters equations from (5.2) - (5.5) becomes as follow:

$$\frac{\partial u}{\partial x}+\frac{1}{r}\left(\frac{\partial (rv)}{\partial r}\right)=0,$$

$$Re\delta\left(\frac{\partial u}{\partial t}+u\frac{\partial u}{\partial x}+v\frac{\partial u}{\partial r}\right)=-\frac{\partial p}{\partial x}+\frac{N}{1-N}\frac{1}{r}\frac{\partial (rw)}{\partial r}+\frac{1}{1-N}\left(\delta^2\frac{\partial^2 u}{\partial x^2}+\frac{1}{r}\frac{\partial}{\partial r}\left(r\frac{\partial u}{\partial r}\right)\right),$$

$$Re\delta^3\left(\frac{\partial v}{\partial t}+u\frac{\partial v}{\partial x}+v\frac{\partial v}{\partial r}\right)=-\frac{\partial p}{\partial r}+\frac{\delta^2}{1-N}\left(-N\frac{\partial w}{\partial x}+\frac{\partial}{\partial r}\left(\frac{1}{r}\frac{\partial (rv)}{\partial r}\right)+\delta^2\frac{\partial^2 v}{\partial x^2}\right),$$

$$\frac{\sigma Re\delta(1-N)}{N}\left(\frac{\partial w}{\partial t}+u\frac{\partial w}{\partial x}+v\frac{\partial w}{\partial r}\right)=-2w+\left(\delta^2\frac{\partial v}{\partial x}-\frac{\partial u}{\partial r}\right)+\frac{2-N}{m^2}\left(\frac{\partial}{\partial r}\left(\frac{1}{r}\frac{\partial (rw)}{\partial r}\right)+\delta^2\frac{\partial^2 w}{\partial x^2}\right).$$

Employing long wavelength and low Reynolds number approximations, the non-dimensional equations obtained from above equations reduce to

$$\frac{\partial u}{\partial x}+\frac{1}{r}\left(\frac{\partial (rv)}{\partial r}\right)=0, \tag{5.8}$$

$$\frac{\partial p}{\partial x}=\frac{1}{1-N}\left\{\frac{N}{r}\frac{\partial (rw)}{\partial r}+\frac{1}{r}\frac{\partial}{\partial r}\left(r\frac{\partial u}{\partial r}\right)\right\}, \tag{5.9}$$

$$\frac{\partial p}{\partial r}=0, \tag{5.10}$$

$$2w+\frac{\partial u}{\partial r}-\frac{2-N}{m^2}\frac{\partial}{\partial r}\left(\frac{1}{r}\frac{\partial (rw)}{\partial r}\right)=0. \tag{5.11}$$

where $N=\frac{k}{(\mu+k)}$ is the coupling number i.e. a measure of particle coupling with its surroundings $(0\leq N\leq 1), m=\sqrt{\frac{a^2k(2\mu+k)}{\gamma(\mu+k)}}$, is the micro-polar parameter and α,β do not appear in the governing as the micro-rotation vector

is solenoidal, i.e. $\nabla \cdot \overrightarrow{w} = 0$. In the limiting case, $k \to 0$ i.e., $N \to 0$, the governing equations for the micro-polar fluid reduce to the governing equations for Newtonian fluid.

$$h(x, \omega, t) = 1 + bx - \phi\, e^{\omega x} \cos^2 \pi(x - t), \tag{5.12}$$

The boundary conditions imposed on the governing equations are as follow

$$u(x,r,t)\Big|_{r=h} = 0, \qquad v(x,r,t)\Big|_{r=h} = \frac{\partial h}{\partial t},$$

$$v(x,r,t)\Big|_{r=0} = 0, \qquad \frac{\partial u(x,r,t)}{\partial r}\Big|_{r=0} = 0, \tag{5.13}$$

$$w(x,r,t)\Big|_{r=0} = 0, \qquad w(x,r,t)\Big|_{r=h} = 0. \tag{5.14}$$

5.3 Solution of the Problem

Integration of equation (5.9) once with respect to r yields

$$\frac{\partial u}{\partial r} = (1 - N)\frac{r}{2}\frac{\partial p}{\partial x} - Nw + \frac{C_1}{r}, \tag{5.15}$$

Further, integrating equation (5.11) twice with respect to r and also using equation (5.15), we obtained non-homogeneous Bessel equation as:

$$\frac{\partial^2 w}{\partial r^2} + \frac{1}{r}\frac{\partial w}{\partial r} - \left(m^2 + \frac{1}{r^2}\right)w = \frac{m^2}{2 - N}\left\{(1 - N)\frac{r}{2}\frac{\partial p}{\partial x} + \frac{C_1}{r}\right\},$$

The general solution of above equation as follows

$$w = C_2 I_1(mr) + C_3 K_1(mr) - \frac{1}{2-N}\left\{(1-N)\frac{r}{2}\frac{\partial p}{\partial x} + \frac{C_1}{r}\right\}, \tag{5.16}$$

where C_1, C_2, C_3 are arbitrary functions independent of r and $I_1(mr), K_1(mr)$ are respectively the modified Bessel functions of the first and second kind of the first order.

Then applying fourth boundary condition of equation (5.13) and the boundary conditions (5.14). Then equations (5.15) and (5.16) become

$$\frac{\partial u}{\partial r} = \frac{1-N}{2-N}\frac{\partial p}{\partial x}\left\{r - \frac{Nh}{2}\frac{I_1(mr)}{I_1(mh)}\right\}, \tag{5.17}$$

$$w = \frac{1-N}{2(2-N)}\frac{\partial p}{\partial x}\left\{\frac{HI_1(mr)}{I_1(mh)} - r\right\}. \tag{5.18}$$

and further integrating equation (5.17) and applying the no-slip condition of equation (5.13), the axial velocity is found as

$$\begin{aligned} u = \frac{1-N}{2(2-N)}\frac{\partial p}{\partial x}\Bigg\{ & r^2 - (1+bx)(1+bx-\phi e^{\omega x} \\ & - \phi e^{\omega x}\cos 2\pi(x-t)) - \frac{\phi^2 e^{2\omega x}}{4}(1 + 4\cos 2\pi(x-t) + \cos^2 2\pi(x-t)) \\ & + \frac{Nh}{m}\left(\frac{I_0(mh) - I_0(mr)}{I_1(mh)}\right)\Bigg\}, \end{aligned} \tag{5.19}$$

where $I_0(mr)$, $I_0(mh)$ are the modified Bessel functions of the first kind and the zeroth order.

The radial velocity is derived from equation (5.11), by substituting u from equation (5.19) and integrating it once with respect to r. The regularity condition, given in equation (5.13), determines the constant term and gives the radial velocity as

$$v = \frac{1-N}{2(2-N)}\Bigg[\Big\{b + \frac{\phi e^{\omega x}}{2}(2\pi \sin 2\pi(x-t) - \omega\cos 2\pi(x-t) - \omega)\Big\}\frac{\partial p}{\partial x}\Bigg\{rh - \frac{N}{m}\Bigg\{\frac{r}{2}\frac{\partial}{\partial x}\left(\frac{hI_0(mh)}{I_1(mh)}\right) - \frac{I_1(mr)}{m}\frac{\partial}{\partial x}\left(\frac{h}{I_1(mh)}\right)\Bigg\}\Bigg\} - \frac{\partial^2 p}{\partial x^2}\Big\{\frac{r^3}{4} - \frac{rh^2}{2} + \frac{Nh}{mI_1(mh)}\left(\frac{r}{2}I_0(mh) - \frac{I_1(mh)}{m}\right)\Big\}\Bigg], \quad (5.20)$$

In order to get pressure gradient, we apply the radial velocity of the wall, given in equation (5.13), on equation (5.20). This gives

$$h\frac{\partial h}{\partial t} = \frac{1-N}{2(2-N)}\Bigg[\Big\{b + \frac{\phi e^{\omega x}}{2}(2\pi \sin 2\pi(x-t) - \omega\cos 2\pi(x-t) - \omega)\Big\}\frac{\partial p}{\partial x}\Bigg\{H^3 - \frac{Nh}{m}\Bigg\{\frac{h}{2}\frac{\partial}{\partial x}\left(\frac{hI_0(mh)}{I_1(mh)}\right) - \frac{I_1(mh)}{m}\frac{\partial}{\partial x}\left(\frac{h}{I_1(mh)}\right)\Bigg\}\Bigg\} + \frac{\partial^2 p}{\partial x^2}\Bigg\{\frac{h^4}{4} + \frac{Nh^2}{2m^2}\left(2 - \frac{mhI_0(mh)}{I_1(mh)}\right)\Bigg\}\Bigg], \quad (5.21)$$

Integrating of which, with respect to x, yields the pressure gradient as

$$\frac{\partial p}{\partial x} = \frac{8(2-N)}{1-N}$$
$$\left[\frac{C(t) + \frac{\pi\phi}{4}\int_0^x e^{\omega x}\{(2\phi e^{\omega x} - 4(bx+1))\sin 2\pi(x-t) + \phi e^{\omega x}\sin 4\pi(x-t)\}\,ds}{h^4 + \frac{4Nh^2}{m^2}\left(1 - \frac{mhI_0(mh)}{2I_1(mh)}\right)}\right], \quad (5.22)$$

Again integrating it from 0 to x, the pressure difference is obtained as

$$p(x,t) - p(0,t) = \frac{8(2-N)}{1-N}$$
$$\left[\int_0^x \frac{C(t) + \frac{\pi\phi}{4}\int_0^s e^{\omega x}\{(2\phi e^{\omega x} - 4(bx+1))\sin 2\pi(x-t) + \phi e^{\omega x}\sin 4\pi(x-t)\}\,ds_1}{h^4 + \frac{4Nh^2}{m^2}\left(1 - \frac{mhI_0(mh)}{2I_1(mh)}\right)} ds\right], \quad (5.23)$$

Putting $x = l$ in equation (5.23), the pressure difference between the inlet and the outlet of the tube is obtained as

$$p(l,t) - p(0,t) = \frac{8(2-N)}{1-N}$$
$$\left[\int_0^l \frac{C(t) + \frac{\pi\phi}{4}\int_0^x e^{\omega x}\{(2\phi e^{\omega x} - 4(bx+1))\sin 2\pi(x-t) + \phi e^{\omega x}\sin 4\pi(x-t)\}\,ds}{h^4 + \frac{4Nh^2}{m^2}\left(1 - \frac{mhI_0(mh)}{2I_1(mh)}\right)} ds\right], \quad (5.24)$$

where $C(t)$ is a function of t which is evaluated as

$$C(t)=\frac{\frac{8(2-N)}{1-N}\Delta p_l(t)-\int_0^l \frac{\frac{\pi\phi}{4}\int_0^x e^{\omega x}\{(2\phi e^{\omega x}-4(bx+1))\sin 2\pi(x-t)+\phi e^{\omega x}\sin 4\pi(x-t)\}\,ds}{h^4+\frac{4Nh^2}{m^2}\left(1-\frac{mhI_0(mh)}{2I_1(mh)}\right)}dx}{\int_0^l \frac{1}{h^4+\frac{4Nh^2}{m^2}\left(1-\frac{mhI_0(mh)}{2I_1(mh)}\right)}dx}, \quad (5.25)$$

where $\Delta p_l(t)=p(l,t)-p(0,t)$ is the pressure difference between the inlet and outlet of the tube.

The volume flow rate is defined as

$$Q(x,t)=\int_0^h 2ur\,dr,$$

this yields, on performing the integration, the following expression

$$Q(x,t)=\frac{N-1}{4(2-N)}\frac{\partial p}{\partial x}\left\{h^4+\frac{4Nh^2}{m^2}\left(1-\frac{mhI_0(mh)}{2I_1(mh)}\right)\right\}, \quad (5.26)$$

The time-averaged volume flow rate is obtained by averaging the volume flow rate for one time period. This gives

$$\tilde{Q}=\frac{N-1}{4(2-N)}\int_0^1 \frac{\partial p}{\partial x}\left\{h^4+\frac{4Nh^2}{m^2}\left(1-\frac{mhI_0(mh)}{2I_1(mh)}\right)\right\}dt, \quad (5.27)$$

The time-averaged volume flow rate can be given in terms of the flow rate in the wave frame, and also in the laboratory frame, as

$$\begin{aligned}\tilde{Q} =& q + 1 + b^2x^2 - 2bx - (1 - bx)\phi e^{\omega x} + \frac{3}{8}\phi^2 e^{2\omega x},\\ =& Q - 4bx + (2bx + (1 + 2bx)\cos 2\pi(x - t))\phi e^{\omega x}\\ &+ \frac{1}{32}(9 - 4\cos 4\pi(x - t) - 16\cos 2\pi(x - t))\phi^2 e^{2\omega x}, \end{aligned} \tag{5.28}$$

This helps us express the pressure gradient in terms of the time-averaged volume flow rate. With some manipulations equation (5.26) and (5.28) give

$$\frac{\partial p}{\partial x} = \frac{4(2 - N)}{N - 1} \left[\frac{\tilde{Q} + 4bx - (2bx + (1 + 2bx)\cos 2\pi(x - t))\phi e^{\omega x} - \frac{1}{32}(9 - 4\cos 4\pi(x - t) - 16\cos 2\pi(x - t))\phi^2 e^{2\omega x}}{h^4 + \frac{4Nh^2}{m^2}\left(1 - \frac{mhI_0(mh)}{2I_1(mh)}\right)} \right], \tag{5.29}$$

On integration, which yields pressure difference, in terms of the time-averaged volume flow rate, as

$$p(x) - p(0) = \frac{4(2 - N)}{N - 1} \int_0^x \left[\frac{\tilde{Q} + 4bx - (2bx + (1 + 2bx)\cos 2\pi(x - t))\phi e^{\omega x} - \frac{1}{32}(9 - 4\cos 4\pi(x - t) - 16\cos 2\pi(x - t))\phi^2 e^{2\omega x}}{h^4 + \frac{4Nh^2}{m^2}\left(1 - \frac{mhI_0(mh)}{2I_1(mh)}\right)} \right] ds, \tag{5.30}$$

which gives $x = l$ for

$$p(l) - p(0) = \frac{4(2-N)}{N-1} \int_0^l \left[\frac{\begin{array}{c} \tilde{Q} + 4bx - (2bx + (1+2bx)\cos 2\pi(x-t))\phi e^{\omega x} \frac{1}{32}(9 - 4\cos 4\pi(x-t) \\ -16\cos 2\pi(x-t))\phi^2 e^{2\omega x} \end{array}}{h^4 + \frac{4Nh^2}{m^2}\left(1 - \frac{mhI_0(mh)}{2I_1(mh)}\right)} \right] ds, \quad (5.31)$$

5.4 Result and discussions

In sequence to explore the effects of numerous parameters such as coupling number, micro-polar parameter and dilation wave amplitude on swallowing of a micropolar fluid, we plot graphs for local pressure along the axis. The case considered here is free pumping which is attained only by provision zero pressure at the two ends of the oesophagus i.e. $\Delta p_l(t) = 0, (p_l(t) = p(l,t) - p(0,t))$. When a non-Newtonian fluid swallows, practically at a time only one bolus moves in the oesophagus. Therefore, for the descriptive expression, we deal with single bolus swallowing in the oesophagus although it can accommodate as many as three boluses at a time as per our discussion.

The fundamental motive is the pressure distribution along the axis when a bolus travels down the oesophagus towards the cardiac sphincter. Since the mathematical model involves expressions that cannot be integrated by classical methods, the only way out is to go for the numerical solution. Moreover, the values of all the non-dimensional parameters are merely suitable assumptions to facilitate the qualitative investigation.

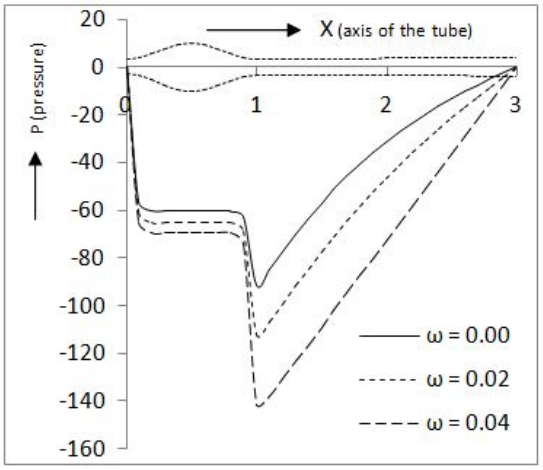

(5.3a) $t = 0.00$

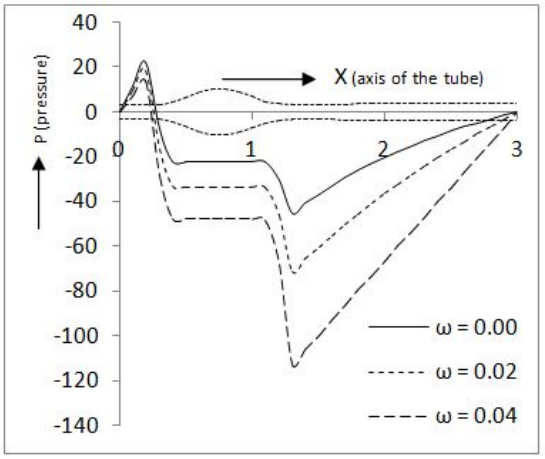

(5.3b) $t = 0.25$

5.4.1 Effect of dilating wave amplitude on pressure

The effect of dilating wave amplitude ω on the flow dynamics is sketched in Figure 5.3. The observation of plot at $t = 0.00$ to $t = 2.00$ (Figure 5.3) show that dissimilar the case of peristaltic wave with constant amplitude (Figures (5.3g)-(5.3i), corresponding to $\omega = 0.00$), the variation between the maximum and the minimum pressures becomes larger when wave-amplitude dilates (Figures (5.3g)-(5.3i), corresponding to $\omega = 0.02$ and $\omega = 0.04$), i.e., pressure distribution for dilating amplitude is observed to differ from that for constant amplitude. An observation of Figures (5.3g) and (5.3i) reveal that pressure gradients, corresponding to $\omega = 0.02$ and $\omega = 0.04$ are greater in magnitude in the lower oesophageal part than that in the upper oesophageal part and also, the pressure rises most in the lower part of the oesophagus. It confirms the experimental observations (Kahrilas *et al*. (1995)) of the high-pressure zone in the lower oesophageal part.

Achalasia causes inadequate lower oesophageal sphincter relaxation. As a consequence of inadequate lower oesophageal sphincter relaxation oesophageal clearance is deferred. Therefore, a possible treatment for patients with inadequate lower oesophageal sphincter relaxation may be that this is overcome through

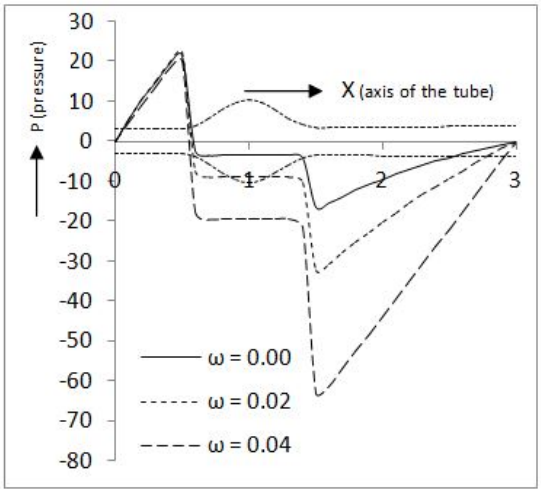

(5.3c) $t = 0.50$

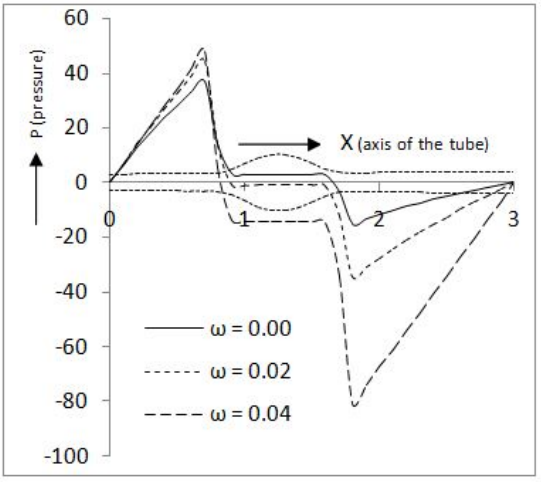

(5.3d) $t = 0.75$

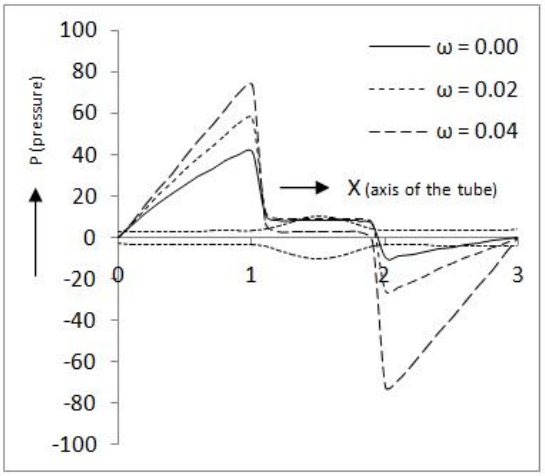

(5.3e) $t = 1.00$

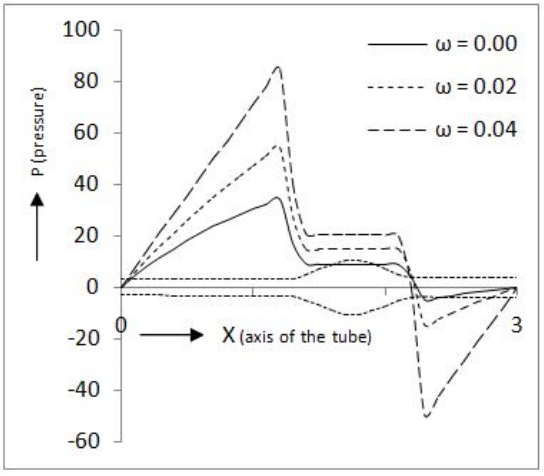

(5.3f) $t = 1.25$

drugs or operation (Spechler and Castell (2001)). Our investigation reveals that swallowing of pseudoplastic fluid requires lesser pressure in compression to that of micropolar fluid or dilatant fluid. Hence, an outcome of the present analysis defends feeding of micropolar fluids for patients suffering from achalasia.

5.4.2 Effect of the gradient parameter on pressure

The effect of the gradient parameter on pressure distribution is shown in Figures 5.4. The pressure is measured at different time instants. We set $\phi = 0.7, \omega =$

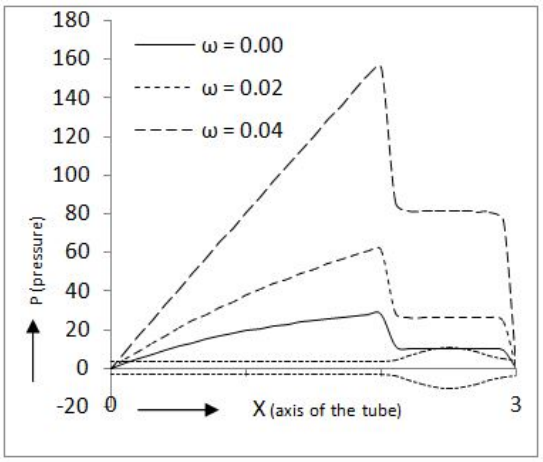

(5.3g) $t = 1.50$

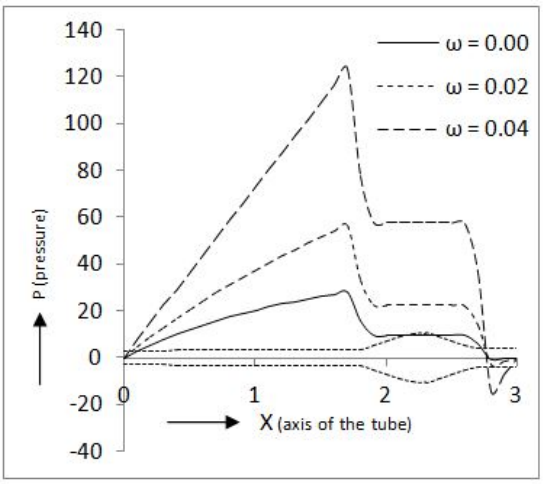

(5.3h) $t = 1.75$

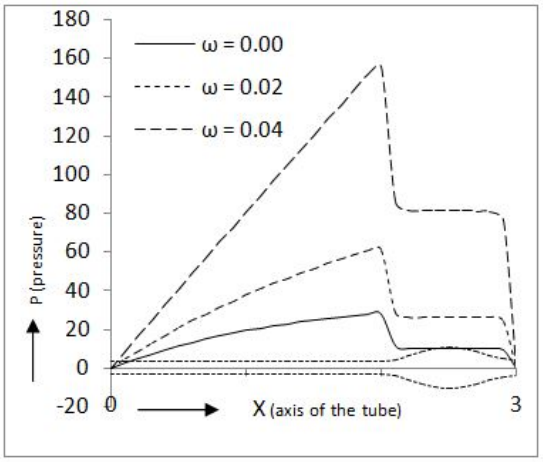

(5.3i) $t = 2.00$

Figure 5.3: ((a)-(i)) Pressure distribution along axial distance at different time instant showing the effect of dilation parameter ω. Other parameters are taken as $l = 3$, $\phi = 0.7$, $N = 0.15$, $m = 1.0$, $b = 0.03$.

0.001, $N = 0.15$, $m = 1.00$ and b is varied in the range $0.00 - 0.04$. At $t = 0.00$ (Figure (5.4a)) it is observed that greater the gradient parameter, lower is the fall in pressure revealing a smaller requirement of pressure. The pressure distribution curves at $t = 0.25$ (Figure (5.4b)) show that the pressure rise, for diverging tube behind the bolus, is greater than that for a uniform tube ($b = 0.00$) but pressure fall is lower than that for a uniform tube. The pressure distribution curve shows

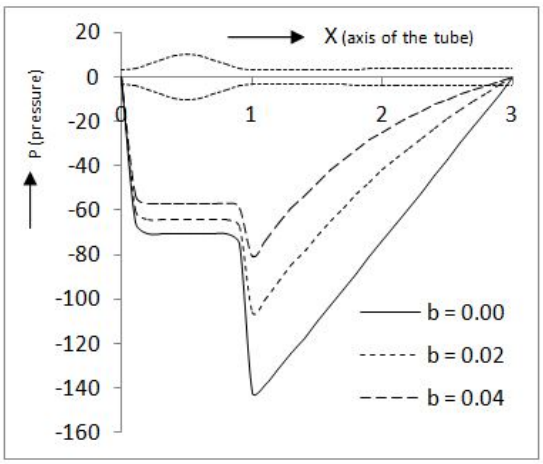

(5.4a) $t = 0.00$

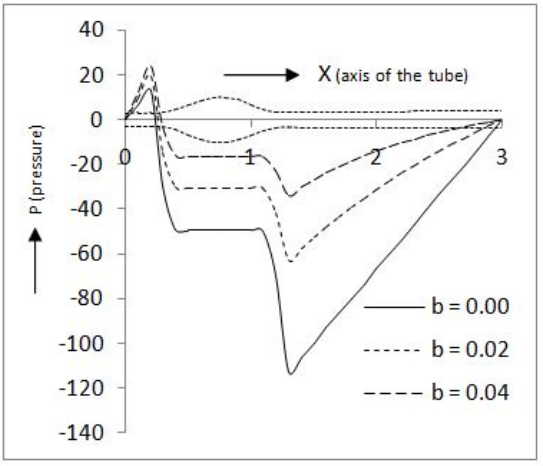

(5.4b) $t = 0.25$

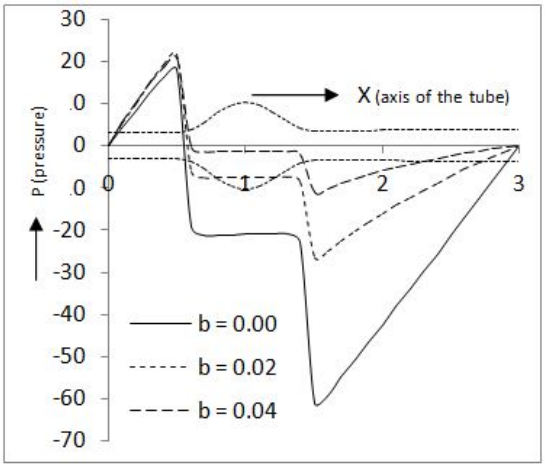

(5.4c) $t = 0.50$

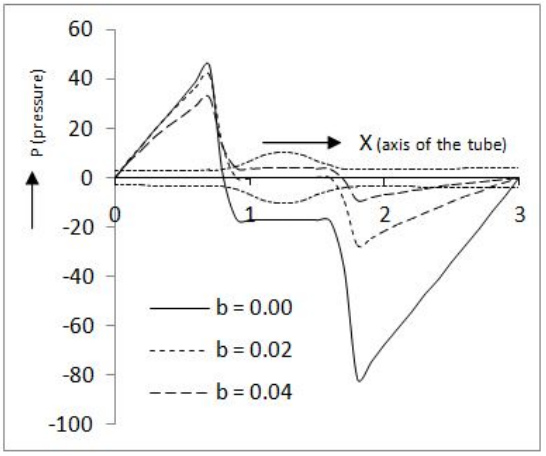

(5.4d) $t = 0.75$

the similar trends at 0.50 (Figure (5.4c)) and $t = 0.75$ (Figure (5.4d)) as the previous. At $t = 1.00$ (Figure (5.4e)) and $t = 2.00$ (Figure (5.4i)), when bolus is situated within the diverged part of the oesophagus, pressure rises here but is less for the diverging tube in comparison to the uniform tube. The comparison of plots at $t = 0.00$ and $t = 2.00$ (Figure 5.4, corresponding to $b = 0.02, 0.04$) show that the difference between the maximum and the minimum pressures becomes smaller when a tube is non-uniform.

In other words for the diverging tube, the upper oesophageal sphincter pressure may be larger than that of lower oesophageal sphincter pressure. When

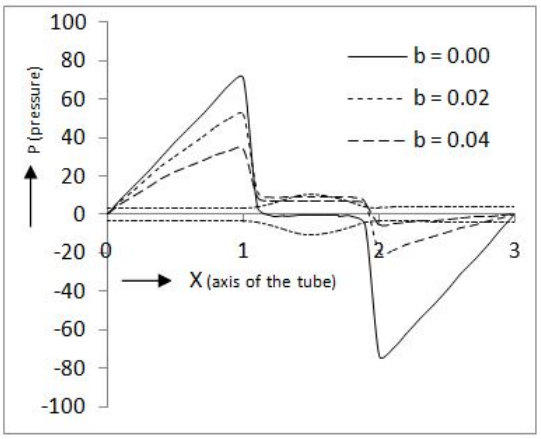

(5.4e) $t = 1.00$

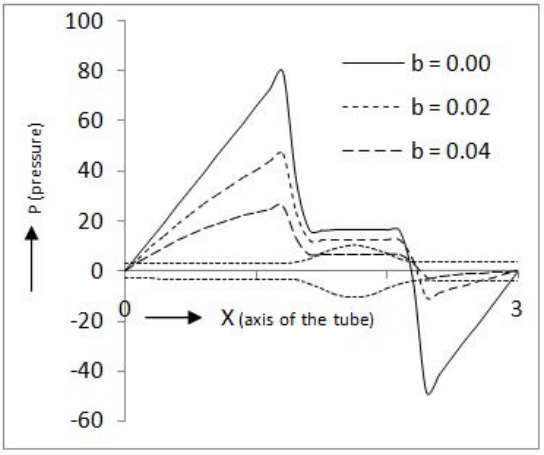

(5.4f) $t = 1.25$

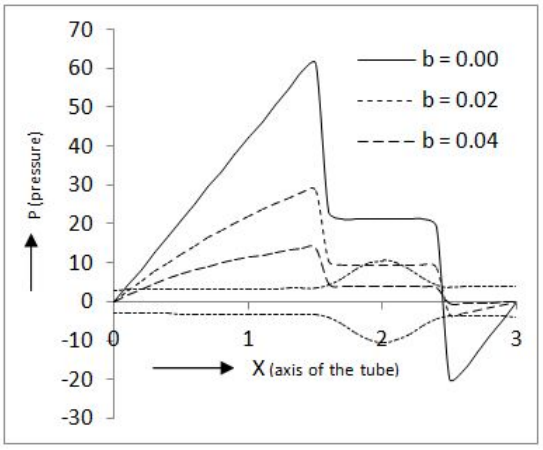

(5.4g) $t = 1.50$

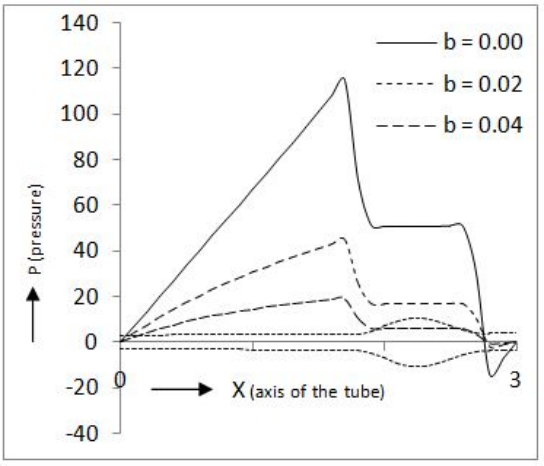

(5.4h) $t = 1.75$

bolus is about to enter in the stomach the pressure rise and fall in the diverging tube are smaller than that in the uniform tube. Therefore, the pressure required to deliver the bolus in the stomach is smaller for diverging oesophagus than that of uniform. The interesting observation is that although tube diverges near the end only, its impact is seen on the pressure distribution right from the beginning of the oesophagus.

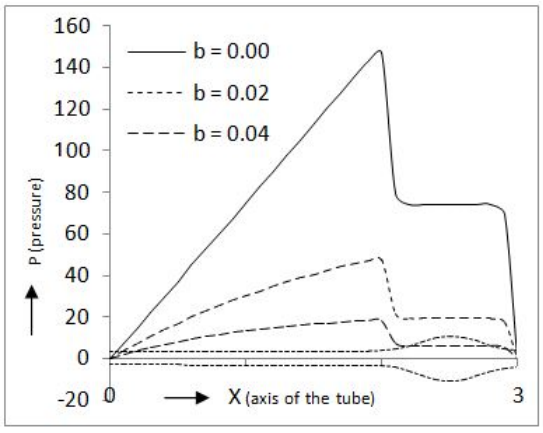

(5.4i) $t = 2.00$

Figure 5.4: ((a)-(i)) Pressure distribution along axial distance at different time instant showing the effect of the gradient parameter b. Other prameters are taken as $l = 3$, $\phi = 0.7$, $\omega = 0.001$, $N = 0.15$, $m = 1.0$

5.4.3 Effect of coupling number on pressure

It also admits that as the coupling effect parameter N increases, pressure gradient, as well as pressure along the length of the oesophagus, magnifies which may be physically explained as that internal rotation of the fluid particles increases pressure; and finally, when $N \to 0$, i.e., the fluids reduce to Newtonian, the pressure is minimum. This may lead to the conclusion that the oesophagus has to make additional efforts to swallow a micropolar fluid. A similar observation is made for all values of t ranging from $0 \to 2$, i.e., throughout one time period. Temporal effects are similar to those observed for Newtonian fluids, power-law fluids, viscoelastic fluids, visco-plastic fluids and magnetohydrodynamic fluids (cf. Hariharan (2008), Pandey (2010)). Figures, together with captions, provide the details (cf. Figure 5.5).

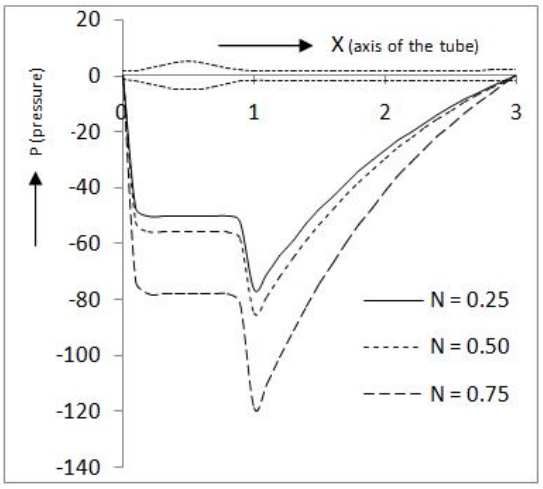

(5.5a) $t = 0.00$

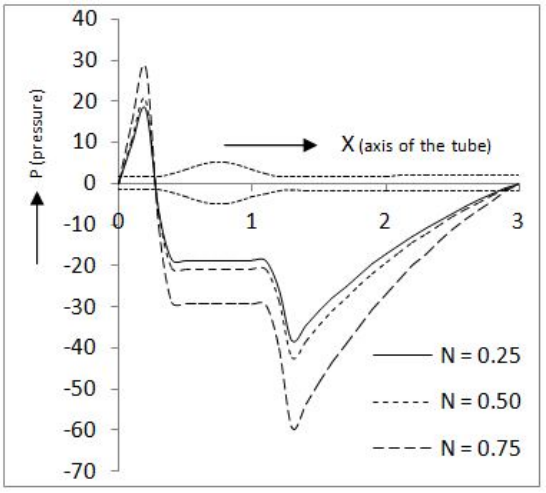

(5.5b) $t = 0.25$

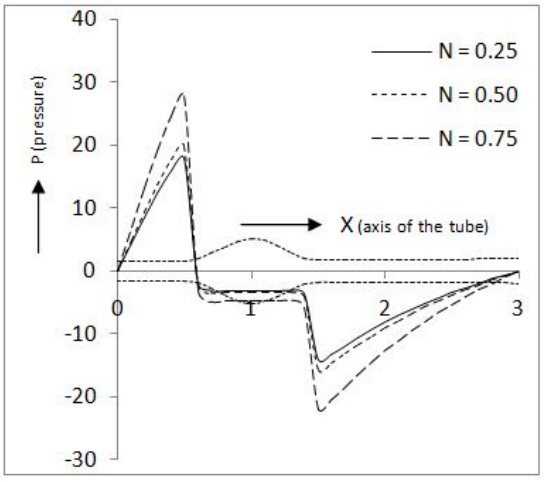

(5.5c) $t = 0.50$

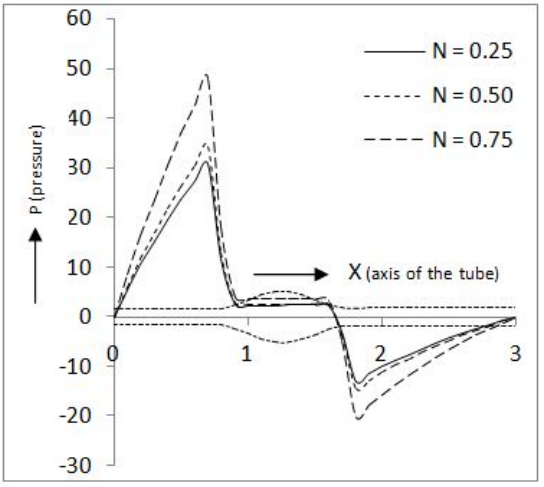

(5.5d) $t = 1.00$

5.4.4 Effect of the micropolar parameter on pressure

We further accomplish analysis into the role of the other micropolar parameter m. It is noticed that the pressure along the entire length of the oesophagus decreases as m increases (cf. Figure 5.6). Hence, this parameter has an opposite effect vis-à-vis coupling number N (cf. Figure 5.5). Since no value of m can leads to Newtonian nature, no comparison can be made with Newtonian fluids. In fact, the micropolar fluid has a complicated characteristic that is built up by the combined effects of these two parameters. This may be recorded that once $N = 0$, m

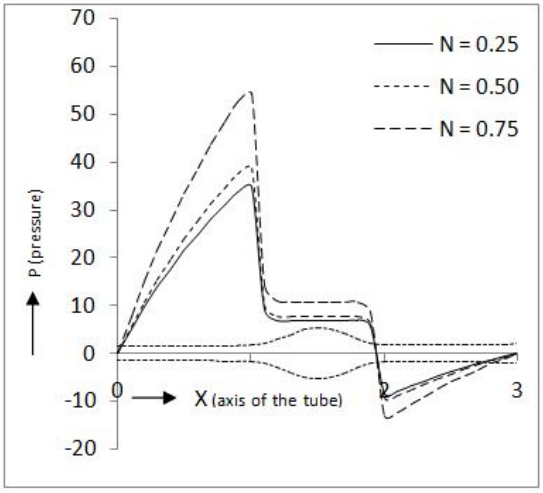

(5.5e) $t = 1.00$

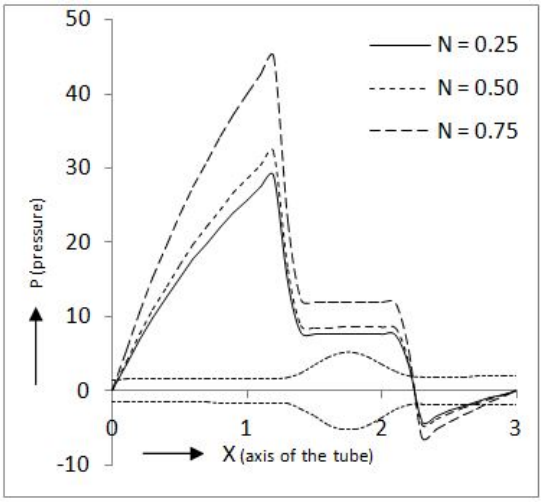

(5.5f) $t = 1.25$

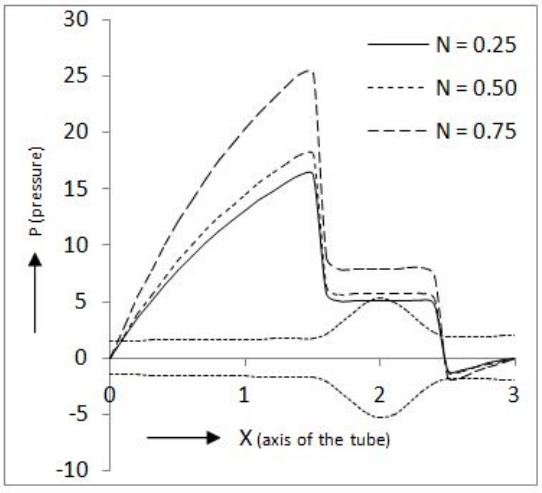

(5.5g) $t = 1.50$

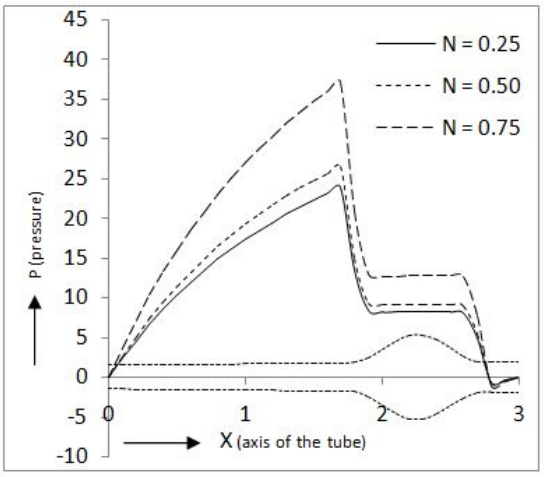

(5.5h) $t = 1.75$

holds to disturb the flow (cf. Equation (5.23)).

5.5 Conclusion and physical interpretations

The objective of this analysis is to pick up the effect of dilating wave amplitude on the nature of the non-Newtonian fluid. Which is flowing in the oesophagus. Here, the non-Newtonian nature is characterized by the micropolar parameter and coupling number. All these characteristics give it the name micro-polar fluid. The

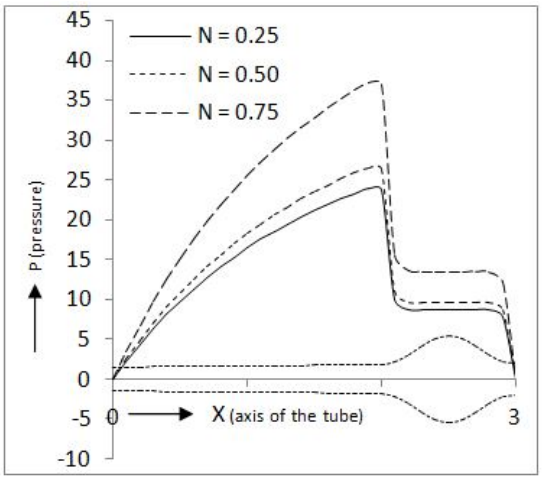

(5.5i) $t = 2.00$

Figure 5.5: ((a)-(i)) Pressure distribution along axial distance at different time instant showing the effect of coupling number N. Other paremeters are teken as $l = 3$, $\phi = 0.7$, $\omega = 0.001$, $m = 1.0$, $b = 0.03$

presence of coupling number and micro-polar parameter requires more pressure to be exerted by the oesophagus wall on the fluid swallowing inside it. Dragging by the dilating wave amplitude increases it further. This confirms the experimental observations (Kahrilas *et al*. (1995)) of high-pressure zone in the lower part of the oesophagus.

The micro-polar and Newtonian fluids have qualitatively identical pressure distributions, but differences in magnitudes are very much significant. The acknowledgement is that coupling number N and dilation parameter ω increases pressure along the entire length of the oesophagus, while the other micro-polar parameter m and gradient parameter b decrease it.

It is also noticed that the magnitude of pressure along the oesophagus increases with increasing coupling number which reveals that swallowing of micropolar fluid is easier than that of dilatant fluid. It is also observed that for exponentially increasing wave-amplitude, pressure keeps increasing along the entire length of the oesophagus; and finally, towards the end of the oesophageal flow,

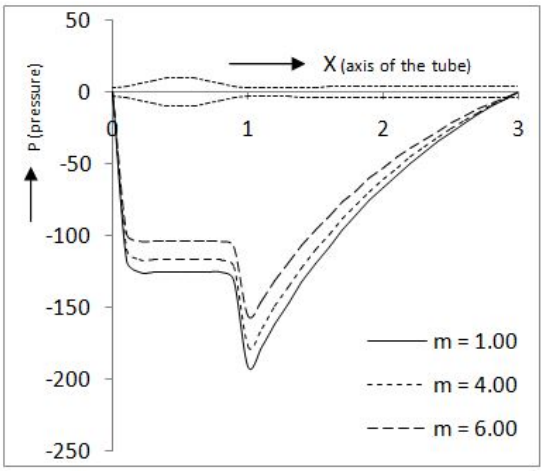

(5.6a) $t = 0.00$

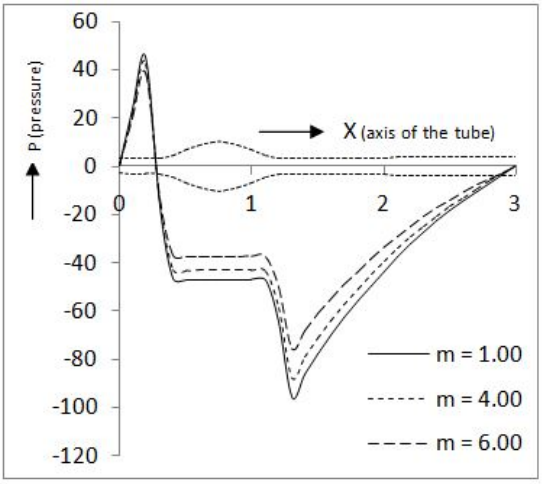

(5.6b) $t = 0.25$

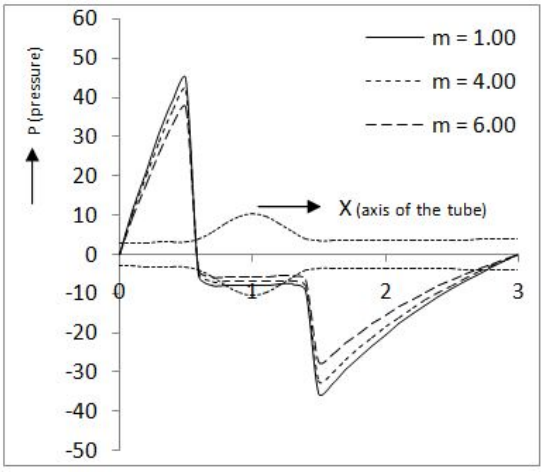

(5.6c) $t = 0.50$

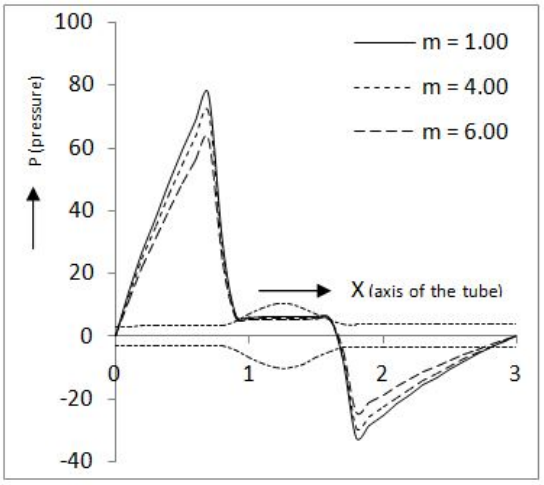

(5.6d) $t = 0.75$

it is at the peak level. It is observed that the pressure distribution is dependent on the position of the wave that propagates in the oesophagus. The local rate of change in the pressure difference is found to be much greater when the wave originates at the inlet and terminates at the outlet of the oesophagus than when the wave travels in the middle (Figures 5.3 - 5.6). This may be associated with the fact that the pumping action does not take place along the entire length of the oesophagus uniformly. The rate of change is higher in the proximity of the inlet and the outlet. It is further concluded that the pressure difference at a given axial position is higher for a dilatant fluid than that for a pseudoplastic fluid. The

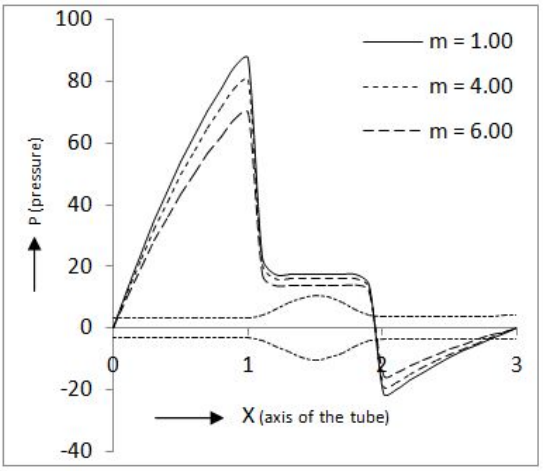

(5.6e) $t = 1.00$

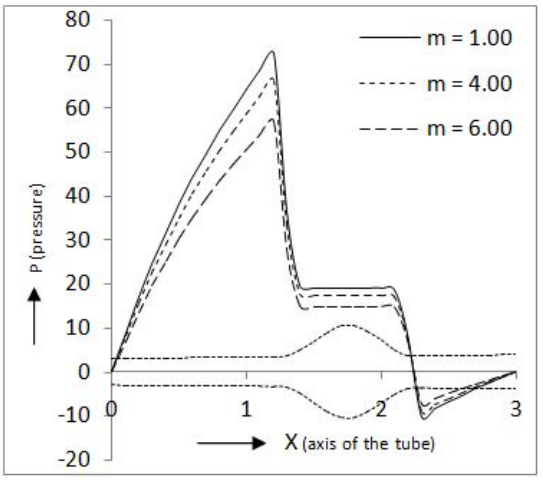

(5.6f) $t = 1.25$

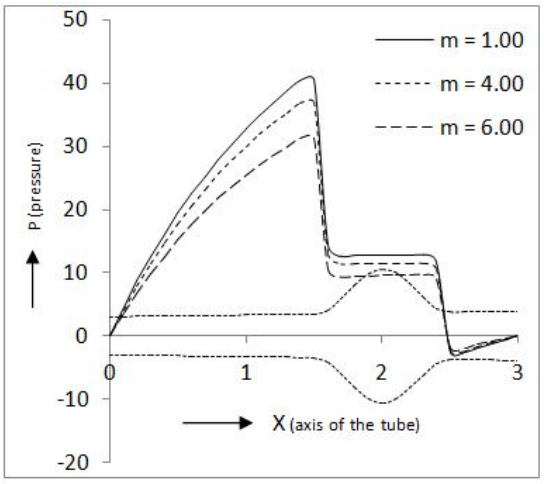

(5.6g) $t = 1.50$

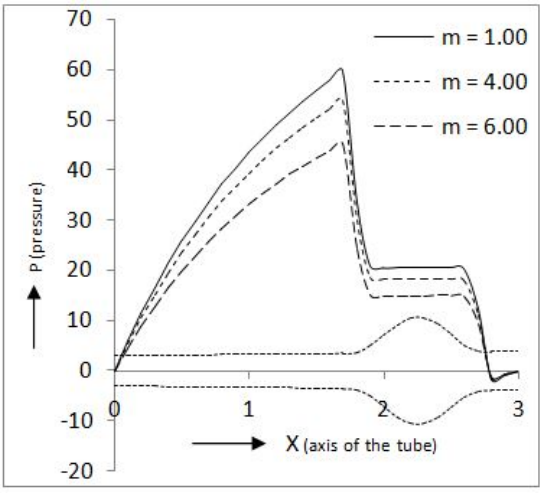

(5.6h) $t = 1.75$

pressure-difference corresponding to a Bingham fluid falls in between these two values. This is also achieved on the basis of the present investigation that feeding of micropolar fluids is preferable to the patients suffering from achalasia.

****

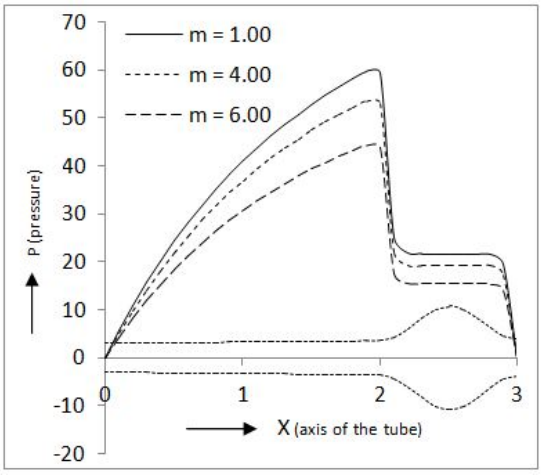

(5.6i) $t = 2.00$

Figure 5.6: ((a)-(i)) Pressure distribution along axial distance at different time instant showing the effect of Micropolar parameter m. Other parameters are taken as $l = 3$, $\phi = 0.7$, $\omega = 0.001$, $N = 0.50$, $b = 0.03$